Journal of Materials Chemistry A

Accepted Manuscript

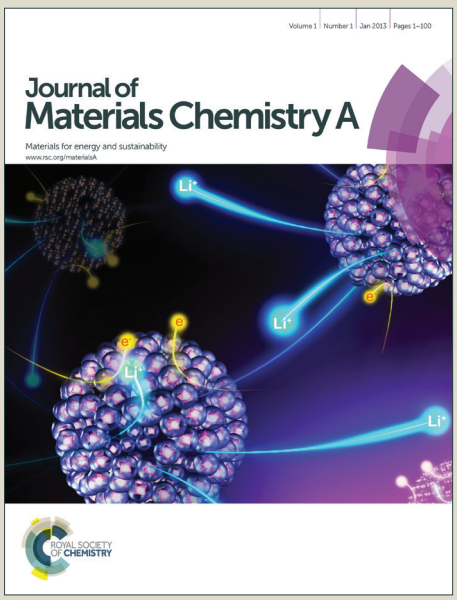

ROYAL SOCIETY OF CHEMISTRY

www.rsc.org/materialsA

Table of Contents

A type-II semiconductor (ZnO/CuS Heterostructure) for visible light photocatalysis

Mrinmoyee Basu[a], Neha Garg[a] and Ashok K. Ganguli[a,b]*

[a] Department of Chemistry, Indian Institute of Technology, Hauz Khas, New Delhi 110016, India

[b] Institute of Nano Science and Technology, Mohali, Punjab 160062, India

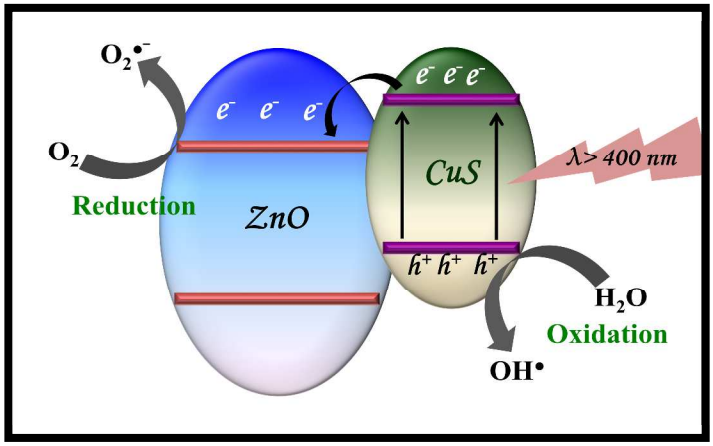

Formation of ZnO/CuS heterostructure through simple wet-chemical method leads to type-II semiconductor. Heterojunction between these two moieties leads the separation of electron hole pair which further enhances the photocatalytic efficiency of ZnO.

A type-II semiconductor (ZnO/CuS Heterostructure) for visible light photocatalysis

Mrinmoyee Basu[a], Neha Garg[a] and Ashok K. Ganguli[a,b]*

[a] Department of Chemistry, Indian Institute of Technology, Hauz Khas, New Delhi 110016, India

[b] Institute of Nano Science and Technology, Mohali, Punjab 160062, India

Abstract:

Type-II semiconductor with p-n heterojunction has been fabricated by decorating CuS nanostructure on the surface of ZnO nanotubes with the help of wet-chemical method at low temperature. We are reporting enhanced visible light photocatalytic efficiency of ZnO/CuS heterostructure. CuO nanostructures have been synthesized on the surface of ZnO nanotubes and then CuO nanostructures were converted to CuS at 80 $^{\circ}$C to generate ZnO/CuS heterostructure. These ZnO/CuS heterostructures efficiently decompose methylene blue upon irradiation of visible light in room temperature. Study of the mechanism suggests that the enhanced photocatalytic activity is due to the formation of ZnO/CuS junction, which leads to efficient separation of photo induced carriers.

Introduction:

In materials chemistry one-dimensional (1D) semiconductor nanostructures have drawn huge attention due to their high surface area, catalytic efficiency, and high electron mobility.[1-3] 1D nanostructures includes nanorods, nanotubes, nanobelts, and nanowires which can efficiently transport electrons and finds their potential application in the field of nanoelectronics, photovoltaics and photocatalysis. 1D nanostructures of different semiconductors have been widely used as photocatalyst due to efficient light-induced charge separation and transport. ZnO is a wide band gap semiconductor material having band gap of 3.37 eV.[4,5] Due to its chemical and mechanical stability and environmental benign character, ZnO has been widely studied and applied in various fields like light-emitting diodes, field-effect transistors, ultraviolet lasers, chemical sensors, solar cells etc.[6,7] Wide applicability in different fields promots scientists to develop several methods for the synthesis of various architectures of ZnO. Among all those techniques, vapor-phase transport, pulsed laser deposition, chemical vapor deposition, wet-chemical method, hydrothermal method and electrochemical deposition have been widely studied for the preparation of 1D ZnO nanostructure.[8-10]

There are several issues that limit the utilization of pure ZnO nanorods for photocatalytic applications. The main drawback of ZnO is that it can only be activated in presence of UV- light. Sunlight radiates only 5% UV light which restricts the applications of ZnO. To widen the applicability of ZnO, different strategies have been employed.[11,12] Metal nanoparticles like Ag, Au, Pt have been decorated on the surface of ZnO, which increases the efficiency of ZnO by delaying the recombination rate of the photo generated electron hole pair.[13-15] To extend the photo response of ZnO, semiconductors having narrow band gap like CdS, PbS, In_2S_3 and Bi_2S_3 have been attached on the ZnO surface to make suitable heterojunctions (band gap engineering) and these heterostructures are applicable in visible light photocatalysis.[16-18] There are very few reports on the surface modification of ZnO by CuS. CuS is a narrow band gap semiconductor (2.2 eV) and is a very suitable candidate for visible light photocatalysis without having any toxic element.[19,20] Gong et al. have synthesized ZnS/CuS porous nanosheets and applied it for visible light photocatalysis for hydrogen production.[21] Yu et al. have synthesized ZnS/CuS hollow heterostructures through ion exchange method and finally they have applied it in visible light photocatalysis.[22] There are some reports on TiO_2/CuS synthesis[23] but few reports are there on the

synthesis of ZnO/CuS heterostructure. Yong et al. have synthesized CuS/ZnO nanoarrays on stainless steel mess and applied it for visible light photocatalytic decomposition of Acid Orange 7.[24] It shows ~80% decomposition of dye molecule in 5h. But the exact mechanism for the enhancement of photocatalytic activity of ZnO/CuS and the band alignment of ZnO and CuS has not been discussed earlier. Basak et al. have synthesized core-shell n-p heterojunction of ZnO and CuS as thin film.[25] They have shown that the ZnO/CuS structure shows an ultrafast photo response speed which will make the material applicable in photodiode. Zhang et al. have synthesized ZnO/CuS composite film and the tribilogical effect of CuS addition in ZnO thin film was investigated.[26]

Being inspired by these previous reports here we have synthesized ZnO/CuS 1D heterostructure following a simple wet-chemical methodology. First we have synthesized ZnO nanotubes and applying these ZnO nanotubes as seed for the synthesis of ZnO/CuO heterostructure. Second, ZnO/CuS heterostructure has been synthesized using as-synthesized ZnO/CuO. In this work we are first time reporting the synthesis of 1D heterostructure of ZnO/CuS. The photocatalytic property of the ZnO/CuS heterostructure has been investigated upon irradiation of visible light. ZnO/CuS 1D heterostructure has shown higher photocatalytic activity than earlier reports. The photocatalytic efficiency of 1D ZnO/CuS heterostructure is very novel and was not studied earlier. Depending on the band energy alignment of ZnO and CuS, formation of type-II semiconductor or p-n heterojunction has been discussed.

Results and Discussion:

Phase purity and crystallinity of the as-prepared ZnO, ZnO/CuO and ZnO/CuS samples were checked with the help of powder x-ray diffraction (PXRD) analysis. Thermodynamically stable phase of ZnO is wurtzite. Figure 1 shows the typical PXRD pattern of ZnO which crystallizes in hexagonal system and the refined cell parameters are a = 3.2515(2) Å and c = 5.2063(8) Å. There is no impurity peak due to $Zn(OH)_2$, un-hydrolyzed Zn(II)-acetate. ZnO/CuO heterostructure has been synthesized applying ZnO tube as seed. PXRD pattern of ZnO/CuO heterostructure shows the characteristic peaks of both ZnO and CuO. From the PXRD pattern it is clear that CuO crystallizes in monoclinic system. ZnO/CuO heterostructure was further utilized as a precursor for the synthesis of ZnO/CuS heterostructure. PXRD pattern of ZnO/CuS

shows the peaks of both ZnO and CuS. So the as-synthesized compound is composed of both hexagonal CuS and ZnO.

Structural Characterization:

Morphology of the as prepared ZnO nanostructure was analyzed with the help of field emission scanning electron microscopy (FESEM). Figure 2 shows the FESEM images of ZnO samples in different magnifications. Low magnification image of ZnO shows that the sample is composed of only ZnO tubes having uniform shape and size. The average length of the ZnO tubes was measured from the side view of the FESEM images. Pure hexagonal ZnO tubes having average length 2.5 μm are formed applying the above described method. Top view of the FESEM images show that hexagonal faces of ZnO tubes have average edge length of 250 nm. These ZnO tubes were used as seeds for the synthesis of ZnO/CuO heterostructure applying a simple wet-chemical method. FESEM images of ZnO/CuO shows that the smooth surface of ZnO tubes has been fully covered with particles of CuO (Figure 3a). From these ZnO/CuO heterostructures ZnO/CuS was synthesized. FESEM images of ZnO/CuS heterostructure shows that smooth surface of ZnO have been covered with CuS nanostructure (Figure 3b).

The element mappings of Zn, O, Cu and S for the selected area (Supporting Information fig.S1) measured by the EDS technique are shown in Fig. S1(b to d). The signals for Zn, O, Cu and S are very uniform, indicating the homogeneous distribution of CuS and ZnO in the heterostructure.

Morphology of ZnO, ZnO/CuO and ZnO/CuS has been examined with the help of TEM analysis. Figure 4 shows the TEM images of ZnO tubes in two different magnifications having length in micrometer region and the contrast in the TEM image of ZnO shows that interior of the tube is completely hollow in nature. TEM image of ZnO nanotubes are in good agreement with the FESEM images. TEM image of ZnO/CuO heterostructure has been shown in Figure 5. Nanotubes of ZnO are fully covered with a layer of CuO nanowires which have grown on the surface of ZnO nanotubes. Figure 6 shows the TEM image of ZnO/CuS heterostructure in different magnifications. Tiny plates of CuS are stacked on the surface of ZnO generating a porous morphology (Figure 6). The formation of core/shell heterostructure was evidenced from the contrast of the core and shell region of ZnO/CuS and ZnO/CuO in the TEM image.

Optical absorption of the as-synthesized ZnO tube, ZnO/CuS heterostructure and bare CuS was determined with the help of UV-visible spectrophotometer at room temperature.

Significant absorption at 370 nm has been assigned for the absorption by ZnO nanotubes (figure 7). According to the equation $\alpha E_p = K(E_p - E_g)^{1/2}$, based on the direct transition a plot of $(\alpha E_p)^2$ vs. E_p gives a curve and the extrapolated value of Ep at $\alpha = 0$ gives absorption edge energies corresponding to band gap E_g of different materials. Using this equation the band gap energy of ZnO nanotube has been calculated which is 3.4 eV and the plot has been shown in supporting information (Fig. S2). This calculated band gap value of ZnO nanotube is relatively higher than that of the bulk ZnO. ZnO/CuS heterostructure clearly shows a broad absorption band in the region 400 to 600 nm. CuS has not been incorporated into the lattice of ZnO, only deposited on the surface of ZnO tube. Using the above stated empirical formula the band gap of CuS has been calculated (Fig.S2) to be 2.67 eV for further determination of the conduction band energy of CuS.

Photocatalysis:

The photocatalysis experiment has been performed in presence of ZnO/CuS as catalyst taking methylene blue as organic pollutant. Methylene blue has a characteristic absorbance peak at 663 nm which has been used to monitor the photocatalytic decomposition. For the performance of the photocatalysis of ZnO/CuS 20 mg of the catalyst and 50 ml 2×10^{-5} M methylene blue has been exploited. Methylene blue does not degrade under irradiation of visible light without using any catalyst(Fig.S3). Similarly ZnO also does not show any photocatalytic performances under irradiation of visible light as it does not absorb visible light. Methylene blue decomposition rate for the case of pure CuS reaches 63% after 30 minute upon irradiation of visible light. It was observed that the photocatalytic efficiency was increased upto 87% dye in 30 min when ZnO/CuS heterostructure was used as photocatalyst(Figure 8). This photocatalytic performance of ZnO/CuS is far better than the earlier reported values.[24] In the equilibrium (dark) there is a large decrease in the concentration of methylene blue which is attributed due to the adsorption of the dye on the catalyst surface. The percentages of degradation of methylene blue dye in presence of ZnO, CuS and ZnO/CuS were 0.6, 63 and 87% respectively after irradiation of visible light in 30 min (Figure 9). The rate constant 'k' value was determined for the different sets of photocatalysis (Figure 8d). In case of pure CuS the value of k is 9.8×10^{-3}min^{-1} whereas when ZnO/CuS has been used as photocatalyst the value of 'k' increases three times to 2.3×10^{-2} min^{-1}. TEM image of the ZnO/CuS heterostructure gives the indication of the stacking of small

plates of CuS on the surface of ZnO which finally leads to a porous structure. Due to such a porous hierarchical structure 72% dye was adsorbed on the surface of the catalyst. Finally upon irradiation of light the adsorbed dye degrade fully.

Effect of reactive species:

There are different reactive species like hydroxyl radical ($OH^{\bullet}$), superoxide radical ion ($O_2^{\bullet -}$) which are generated in the photocatalysis process. These radicals are reactive intermediates and are generated upon reaction of electrons and holes with H_2O separately. So, the main reactive species are electrons and holes. To get an in-depth knowledge of the mechanistic pathway of photocatalysis in different scavenging environment was studied. From literature it has been unveiled that $AgNO_3$ and ammonium oxalate can act as good electron and hole scavenger.[27] So, in our case $AgNO_3$ and ammonium oxalate has been employed as electron and hole scavenger. Prior to the addition of the catalyst in the solution of methylene blue, hole and electron scavengers are introduced. Final concentration of the scavengers has been taken as 10^{-3} M.

Figure 10 shows the degradation of methylene blue in presence of the electron scavenger, $AgNO_3$. Immobilization of the Ag^+ ions on the surface of the catalyst hinders the adsorption of cationic methylene blue. As a result of which only 7% of the dye was adsorbed in presence of Ag^+ ion under equilibrium conditions after 20 min in the dark. Finally, it was observed that there was only 53% dye that has been degraded after 30 min and finally reaction was ceased. This indicates that electrons are the most powerful species and actively take part in photocatalysis. Figure 11 shows that in presence of ammonium oxalate the rate of the reaction has been accelerated. Due to the scavenging of the holes, probability of the electron and hole pair recombination diminishes and rate of reaction increases.

Mechanism for Enhanced Photocatalytic activity of ZnO/CuS tubes:

In case of heterogeneous photocatalysis there are two most important steps. Efficient adsorption of dye molecules on the catalyst surface and successive decomposition of the dye molecule by reaction with the photogenerated electron and hole seperately.[28] In our present case hierarchical morphology of the ZnO/CuS heterostructure and the negative surface charge of the sample leads to enhanced adsorption of the cationic dye methylene blue on the catalyst surface.

p-n heterojunction forms between nanotubes of ZnO and CuS nanostructure. Due to the formation of the heterostructure, there is the successive electron injection from p-type CuS

semiconductor to n-type ZnO upon irradiation of visible light as the conduction band energy of ZnO is lower than that of CuS. Successive charge injection form the conduction band (C. B) of CuS to C. B of ZnO leads to the higher charge carrier separation[29] and higher rate of decomposition of methylene blue on the surface of ZnO/CuS under irradiation of visible light. Effective charge separation can be explained by the band energy alignment of ZnO and CuS. With help of the empirical formula, [30]

$$E_{CB} = -A$$

$$\text{Or, } E_{CB} = -X + 1/2\ E_g$$

$$E_{VB} = E_{CB} - E_g$$

valence and conduction band energy of ZnO and CuS have been calculated. In the given equation E_{CB} is the conduction band edge potential, X is the electro negativity of the semiconductor, which is the geometric mean of the electronegativity of the constituent atoms, and Eg is the bandgap energy of the semiconductor**.** The electro negativity of ZnO and CuS obtained are 5.79 and 5.27.[30] Using these electronegativity values, the conduction band energy of ZnO and CuS were found to be -4.02 eV and -3.89 eV applying the Eg value of ZnO and CuS was 3.37 eV and 2.76 eV respectively.

$$CuS/ZnO + h\nu \xrightarrow{\lambda > 400\ nm} CuS(h^+)/ZnO(e^-)$$

$$ZnO(e^-) + O_2 \longrightarrow O_2^{\bullet -}$$

$$O_2^{\bullet -} + H_2O \longrightarrow H_2O_2 + OH^{\bullet} \text{---------- (1)}$$

$$H_2O_2 \longrightarrow OH^{\bullet}$$

$$OH^{\bullet} + \text{Organic dye} \longrightarrow CO_2 + \text{Water}$$

Or

$$CuS(h^+) + H_2O \longrightarrow OH^{\bullet} \text{----------(2)}$$

$$OH^{\bullet} + \text{Organic dye} \longrightarrow CO_2 + \text{Water}$$

Visible light irradiation on the ZnO/CuS sample generates electron/hole pair on the surface of CuS. Electrons from the valence band of CuS have been lifted to the conduction band absorbing the excess energy. As, from the earlier calculation it has been observed that conduction band energy of ZnO is lower than that of CuS, there will be switching of electron from the conduction

band of CuS to ZnO. Electrons in the conduction band of ZnO react with dissolved oxygen to give superoxide radical which further reacts with water to give hydroxyl radical.[31] Further this hydroxyl radical reacts with organic dye molecule to degrade (equation 1). Similarly hydroxyl radical also generates upon reaction with holes in the valence band of CuS and water molecule which can also further decompose organic molecule (equation 2).

In our present study heterostructure of ZnO/CuS is showing the best photocatalytic efficiency (2.5 times higher), compared to bare CuS. To get a clear understanding of reasons leading to the enhancement of the photocatalytic performance of ZnO/CuS, we looked at the electrochemical impedance spectroscopy studies. Figure 13 shows the Nyquist plots of the as-prepared ZnO/CuS heterostructure and CuS nanostructure. EIS measurement was conducted in the dark condition. In this study we observed only one semicircle arc in the Nyquist plot. The large semicircle was observed in the dark condition for ZnO/CuS heterostructure which is attributed to the recombination resistance. Recombination resistance related to the recombination of electrons in the interface. The radius of the semicircular arc signifies the recombination resistance.[32] The value of recombination resistance is inversely proportional to the value of recombination rate and density of electrons in the material. In the present case, the recombination resistance of bare CuS is much less than that of ZnO/CuS. Larger recombination resistance means lower the rate of recombination. It means greater number of electron transfer occurs in case of ZnO/CuS in comparison to CuS. Electron transfer from the surface of CuS to ZnO due to the formation of the heterostructure is thus supported by the impedance measurement.

Experimental Section:

All absorption spectra were recorded on a UV-2450 PC Shimadzu spectrophotometer (Kyoto, Japan) in the wavelength range of 200 to 800 nm taking the ethanolic dispersion of the sample in a 1 cm quartz cuvette. Powder X-ray diffraction studies (PXRD) were carried out on a Bruker D8 Advance diffractometer using Ni-filtered Cu Kα radiation. Normal scans were recorded with a step size of 0.02^{o} and step time of 1s. Raw data was subjected to background correction and the $K\alpha_2$- lines were stripped off. The particle size, shape, and morphology of nanoparticles were observed with a field emission scanning electron microscope, FESEM (FEI QUANTA 3D FEG) and an EDS machine attached to the instrument was used to obtain the composition of the product. The nanostructures were observed using a transmission electron microscope (TEM JEOL 2010). For the TEM observations, the powders were dispersed in

ethanol and ultrasonicated for 15 min. A few drops of this solution was taken on a carbon-coated copper grid and dried well. Photocatalysis experiment was carried out in a 100 W tungsten bulb which is emitting visible light only. Electrochemical impedance spectroscopy (EIS) measurements were performed with a computer controlled electrochemical work-station (Metrohm Autolab 302/PGSTAT). The three-electrode cell consists of Ag/AgCl as reference electrode, Pt wire as counter electrode and Glassy carbon as working electrode (0.02 cm^2 nominal planar area). Glassy carbon electrode (GCE) was polished using (0.05 μm) alumina paste, ultrasonicated in distilled water and then in ethanol for the electrochemical impedance spectroscopy studies.

Synthesis of Material:

Synthesis of ZnO tubes:

Following a simple wet-chemical route ZnO nanomaterials was synthesized. First 0.01 M Zn-acetate was taken as the precursor of Zn (II) and to it 0.01 M pyridine was added as hydrolyzing agent. After immediate addition of pyridine there was no color change of the solution. Finally the clear solution was kept at 200 ˚C for 3h. After 3h white precipitate of ZnO was collected and washed thoroughly with ethanol. Product was dried and kept for further characterization.

Synthesis of ZnO/CuO heterostructure:

The as-synthesized ZnO nanomaterial was taken in a conical flask and dispersed in water. Then the aqueous dispersion was ultrasonicated for 30 min to get a complete clear dispersion. After that aqueous solution of 0.1 M $CuSO_4$was added and magnetically stirred for 1h at 80˚C. After successful surface decoration by Cu^{2+}, white ZnO became bluish white, which indicates the surface decoration by metal ion. Then, 0.1 M NaOH was added in the stirring condition and heated at 200 ˚C for 2h. Grey colored precipitate was collected, washed thoroughly and kept for further characterization.

Synthesis of ZnO/CuS heterostructure:

As-synthesized ZnO/CuO heterostructure was taken in a conical flask and dispersed well in water using ultra-sonication. Then to this dispersion 0.01 M thioacetamide was added and

heated at 80 ˚C for 1h. After that the grey colored ZnO/CuO compound was converted to greenish black which was washed with ethanol and collected. Synthesis of ZnO/CuS has been shown in scheme 1.

Photodecomposition of Dye molecule catalyzed by the composite material:

For the determination of the photocatalytic activity of ZnO/CuS heterostructure, methylene blue was chosen as a model pollutant. Photocatalytic activity of ZnO/CuS was monitored by observing the decolorization of the dye. For this process, 20 mg of the catalyst and 50 ml 2×10^{-5} M methylene blue (aqueous solution) were used. In a beaker 50 ml 2×10^{-5} M methylene solution has been taken and then to it 20 mg of catalyst has been added. After addition of the catalyst it was magnetically stirred in dark till the equilibrium reached. After reaching equilibrium the whole solution was irradiated under 100 W tungsten bulb, which emits visible light ($\lambda > 400$ nm) only. The photocatalysis reaction have carried out in neutral pH i.e., pH-7. Photocatalytic efficiencies of bare ZnO, bare CuS and ZnO/CuS heterostructure were monitored. At regular time (irradiation) intervals1.0 ml of aliquot was taken out and centrifuged at 1000 rpm for 1 minute, the dye remaining in solution was quantified by measuring the absorption intensity at 664 nm, which is the wavelength of maximum absorbance of methylene blue. The peak intensity was used to calculate degradation yield (Y). Y was calculated as:

$$Y\ (\%) = (I_0-I_t)/I_0\ X\ 100$$

Where I_0 is the initial peak intensity of MB and I_t is the peak intensity with time 't' in photo-irradiation. To determine the order of the reaction, I_t vs. t was plotted. Finally the value of rate constant was determined from the plot of $\ln I_t$ vs. t.

Deferent scavengers have been exploited to trap photogenerated electrons and holes in photocatalysis. Aqueous solutions of silver nitrate and ammonium oxalate have been used keeping all other condition unaltered.

Impedance Measurement:

A mixture of 5 mg of the catalyst with 5 μL of isopropyl alcohol was prepared by ultrasonication for 30 min and 5 μL of Nafion was added as a binder. Nafion acts as a proton conducting binder for nanoparticles which forms a membrane MEA (membrane electrode assembly) over the

surface of electrode. From the above solution, 2 drops were taken and placed on the glassy carbon electrode and air-dried for 1 h. 1 M KOH was used as an electrolyte and the glassy carbon electrode was placed in the cell containing 40 ml of 1 M KOH solution. For each experiment freshly prepared solutions of KOH was used. All potentials were referred to the reference electrode. All electrochemical measurements were performed at 25 ˚C. EIS measurements were performed by applying an AC voltage with 1 mV amplitude in a frequency range from 0.01 to 100 kHz.

Conclusion:

We have successfully developed a simple wet-chemical method for the decoration of CuS nanostructure on the surface of ZnO nanotubes. This methodology leads to heterojunction between p-type CuS and n-type ZnO. Decoration of CuS on the surface of ZnO leads to increase of absorbance in the visible light and the successful charge separation from CuS to ZnO through hexagonal nanotubes of ZnO leading to the delayed recombination of the electron hole pair. The composite material ZnO/CuS with n-p heterojunctions 2.5 times more efficient as photocatalyst in comparison to the bare CuS. Electrochemical impedance studies confirmed the photocatalytic experiments indicating the ease of electron transfer and the lower resistance in the heterostructure.

Acknowledgements:

The authors are thankful to the DST, UGC, NST, DRDO and CSIR, New Delhi, and IIT Delhi.

References:

1. Z. L. Wang, *ACS Nano* 2008, **2**, 1987.
2. S. Chatterjee, K. Bhattacharyya, P. Ayyu, and A. K. Tyagi, *J. Phys. Chem. C* 2010, **114**, 9424.
3. J-H. Lee, I-C. Leu, M-C. Hsu, Y-W. Chung and M-H. Hon, *J. Phys. Chem. B* 2005, **109**, 13056.
4. Z. Chen, N. Zhang and Y-J. Xu, *Cryst Eng Comm*. 2013, **15**, 3022.
5. P. Leidinger, N. Dingenouts, R. Popescu, D. Gerthsen and C. Feldmann, *J. Mater. Chem*. 2012, **22**, 14551.
6. J. Han, F. Fan, C. Xu, S. Lin, M. Wei, X. Duan and Z. L. Wang, *Nanotechnology* 2010, **21**, 40520.
7. D. Pugliese, F. Bella,V. Cauda, A. Lamberti, A. Sacco, E. Tresso, and S. Bianco, *ACS Appl. Mater. Interfaces* 2013, **5**, 11288.
8. R. Zhu, W. Zhang, C. Li, and R. Yang, *Nano Lett*. 2013, **13**, 5171.
9. S. K. N. Ayudhya, P. Tonto, O. Mekasuwandumrong,V. Pavarajarn, and P. Praserthdam, *Cryst. Growth Des.* 2006, **6,** 2446.
10. J. Choi, H. Ji, O. T. Tambunan, I-S. Hwang, H-S. Woo, J-H. Lee, B. W. Lee, C. Liu, S. J. Rhee, C. U. Jung, and G-T. Kim, *ACS Appl. Mater. Interfaces* 2011, **3**, 4682.
11. H. Park, S. Chang, J. Jean, J. J. Cheng, P. T. Araujo, M. Wang, M. G. Bawendi, M. S. Dresselhaus, V. Bulović, J. Kong, and S. Gradecak□, *Nano Lett*. 2013, **13**, 233.
12. O. Akhavan, *ACS Nano* 2010, **4**, 4174.
13. A. Kim, Y. Won, K. Woo, C-H. Kim, and J. Moon, *ACS Nano* 2013, **7**, 1081.
14. C. Gu, C. Cheng, H. Huang, T. Wong, N. Wang, and T-Y. Zhang, *Cryst. Growth Des*. 2009, **9**, 3278.
15. P. Roy, A. P. Periasamy, C-T. Liang and H-T. Chang, *Environ. Sci. Technol.* 2013, **47**, 6688.
16. Y. Bu, Z. Chen, W. Li, and J. Yu, *ACS Appl. Mater. Interfaces* 2013, **5**, 5097.
17. J. Jean, S. Chang, P. R. Brown, J. J. Cheng , P. H. Rekemeyer, M. G. Bawendi, S. Gradec̆ak, and V. Bulovic, *Adv. Mater.* 2013, **25**, 2790.

18. S. Balachandran and M. Swaminathan, *Dalton Trans*. 2013, **42**, 5338.
19. M. Basu, A. K. Sinha, M. Pradhan, S. Sarkar, Y. Negishi, Govind, and T. Pal *Environ. Sci. Technol.* 2010, **44**, 6313.
20. Y. Zhang, J. Tian, H. Li, L. Wang, X. Qin, A. M. Asiri, A. O. Al-Youbi and X. Sun, *Langmuir*, 2012, **28**, 12893.
21. J. Zhang, J. Yu, Y. Zhang, Q. Li and J. R. Gong, *Nano Lett.* 2011, **11**, 4774.
22. J. Yu, J. Zhang and S. Liu, *J. Phys. Chem. C* 2010, **114**, 13642.
23. Q. Wang, N. An, Y. Bai, H. Hang, J. Li, X. Lu, Y. Liu, F. Wang, Z. Li and Z. Lei, *Int. J. Hydrogen Energy* 2013, **38**, 10739.
24. M. Lee and K. Yong, *Nanotechnology* 2012, **23**, 194014.
25. S. Panigrahi and D. Basak, *RSC Adv.* 2012, **2**, 11963.
26. Y. Zhang, B. Huang, P. Li, X. Wang and Y. Zhang, *Tribol Int.* 2013, **58**, 7.
27. A. Kudo, K. Ueda, H. Kato and I. Mikami, *Catal. Lett.*1998, **53**, 229.
28. Y. Tak, H. Kim, D. Lee and K. Yong, *Chem. Commun.,* 2008, 4585–4587. S. Hotchandani and P. V. Kamat, *J. Phys. Chem*., 1992, **96**, 6834.
29. S. Khanchandani, S. Kundu, A. Patra and A. K. Ganguli *J. Phys. Chem. C*, 2012, **116**, 23653–23662.
30. Y. Xu and M. A. A. Schoonen, *Am. Mineral*. 2000, **85**, 543.
31. T-J. Liu, Q. Wang and P. Jiang, *RSC Adv.,* 2013, **3**, 12662. Y. Wang, Q. Wang, X. Zhan, F. Wang, M. Safdar and J. He, Nanoscale, 2013, **5**, 8326.
32. H. Kim, H. Jeong, T. K. An, C. E. Park and K. Yong, *ACS Appl. Mater. Interfaces* 2013, **5**, 268.

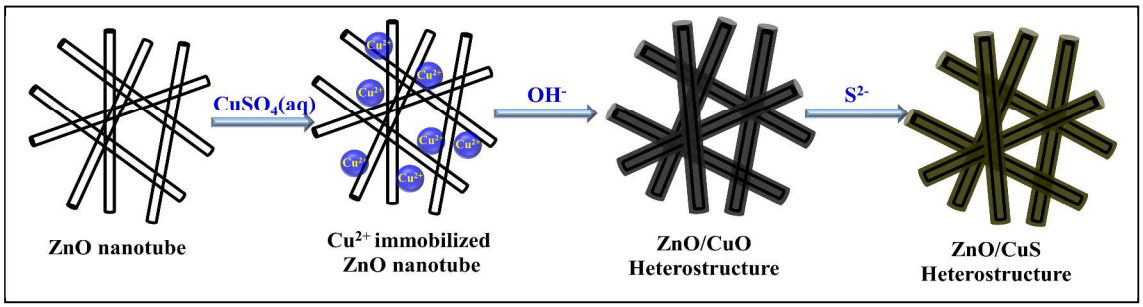

Scheme 1: Schematic representation for the synthesis of ZnO/CuS

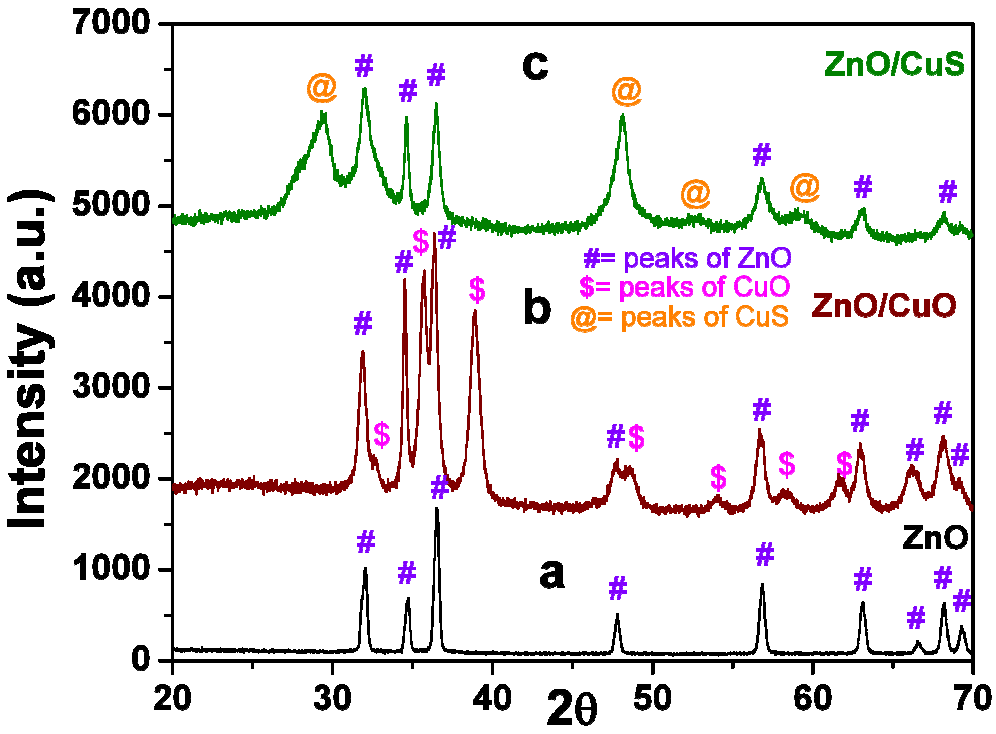

Figure 1: XRD pattern of (a) ZnO, (b) ZnO/CuO and (c) ZnO/CuS.

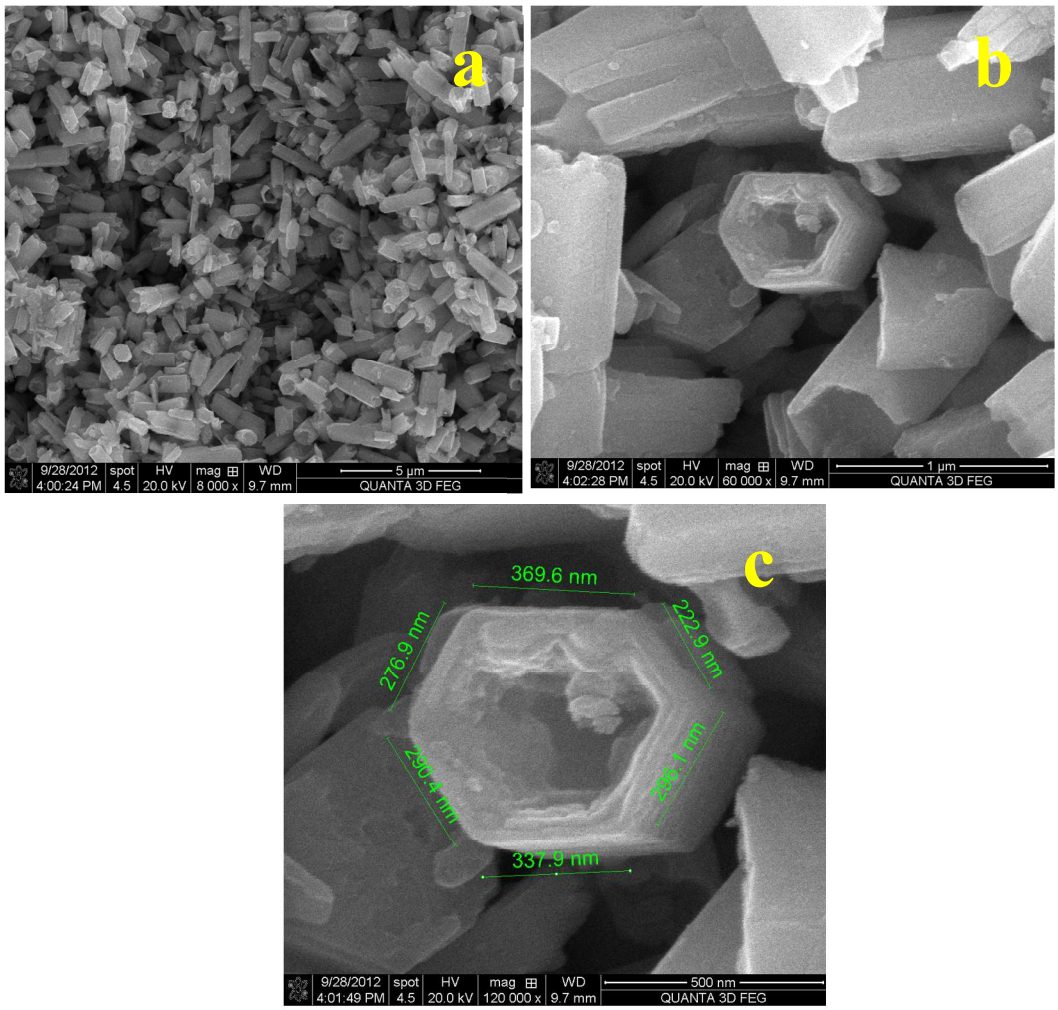

Figure 2: FESEM image of ZnO nanostructures in different magnifications (a) low, (b) medium, (c) high.

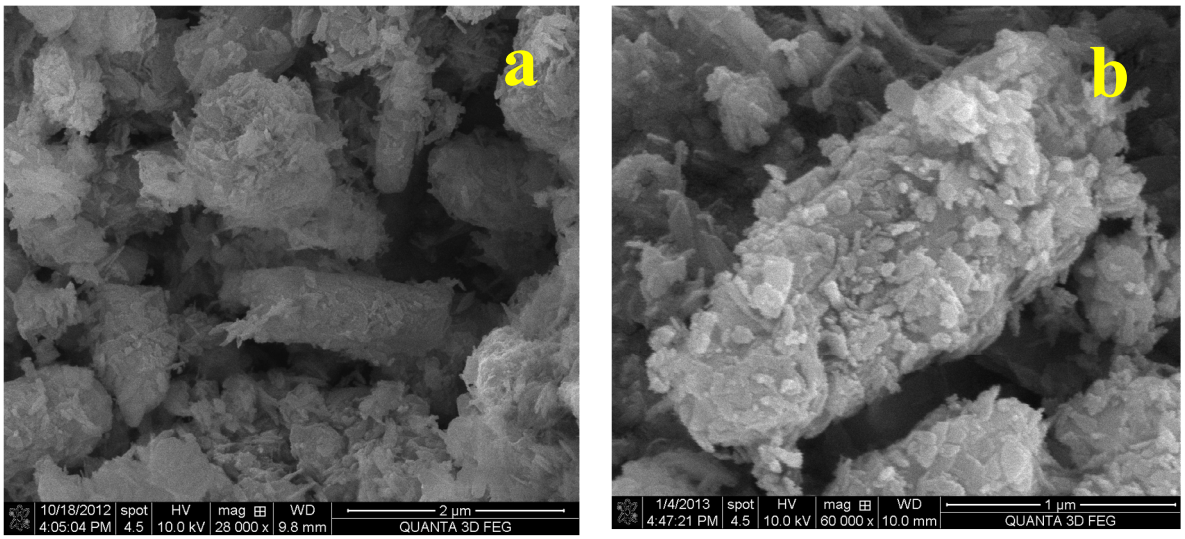

Figure 3: FESEM image of (a) ZnO/CuO heterostructure and (b) ZnO/CuS heterostructure.

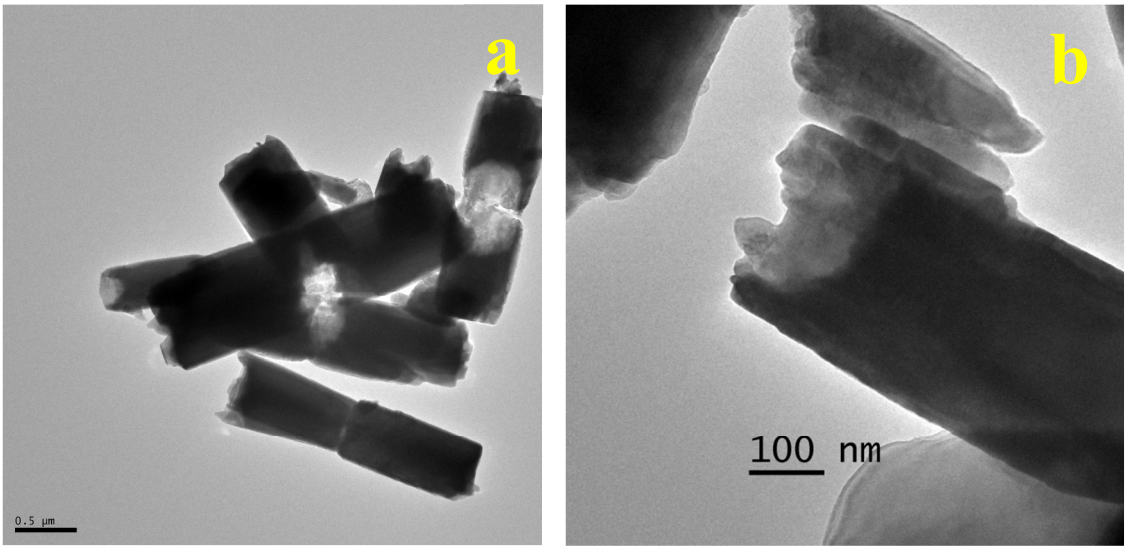

Figure 4: TEM image of ZnO nanotubes in different magnifications (a) low, (b) high.

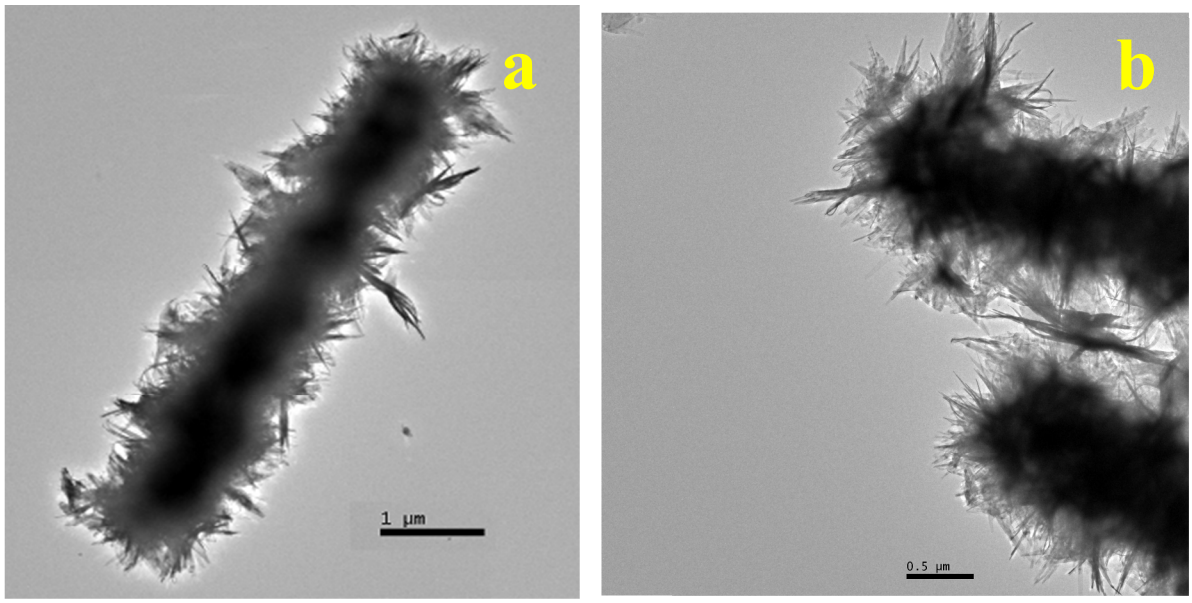

Figure 5: TEM image of ZnO/CuO heterostructure in different magnifications (a) low and (b) high.

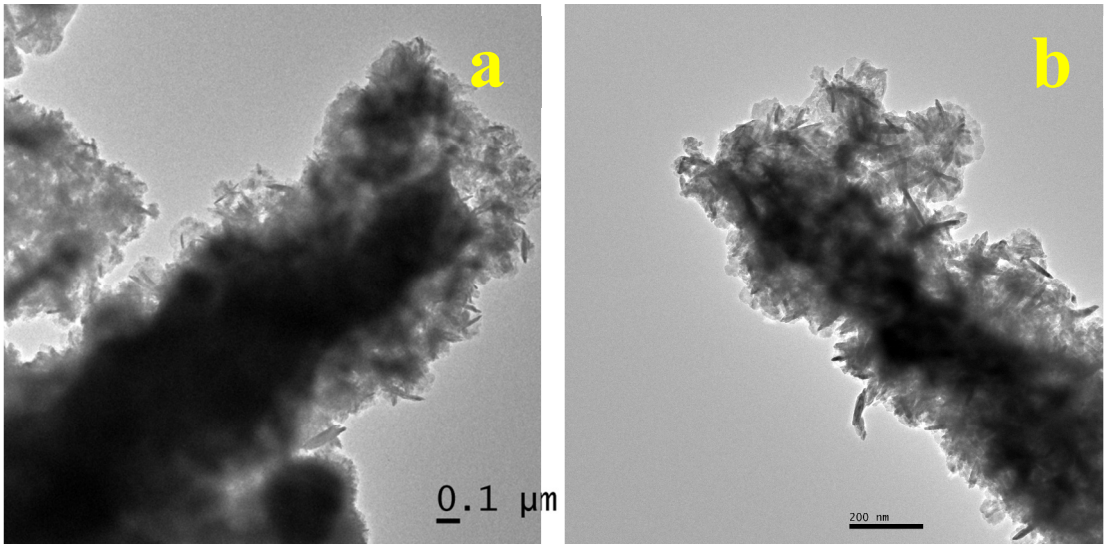

Figure 6: TEM image of ZnO/CuS heterostructure in different magnifications (a) low and (b) high.

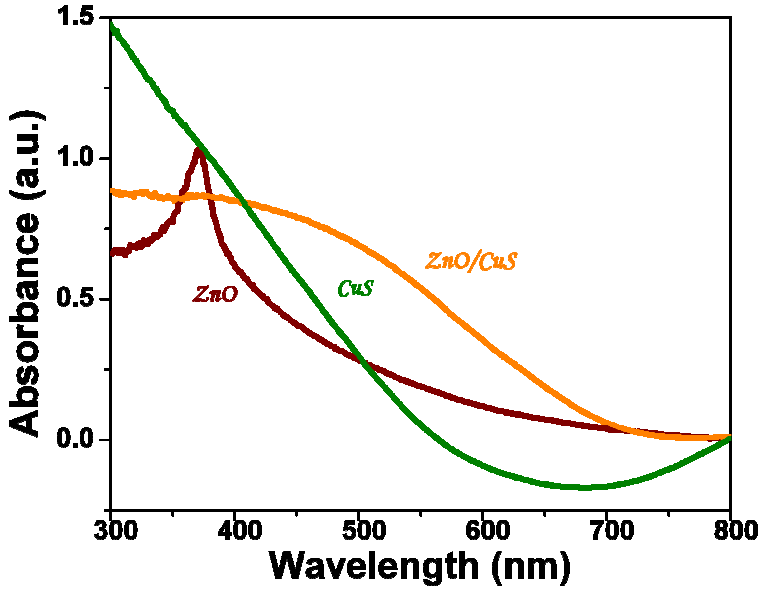

Figure 7: UV-visible spectra of bare ZnO, CuS, ZnO /CuS heterostructure.

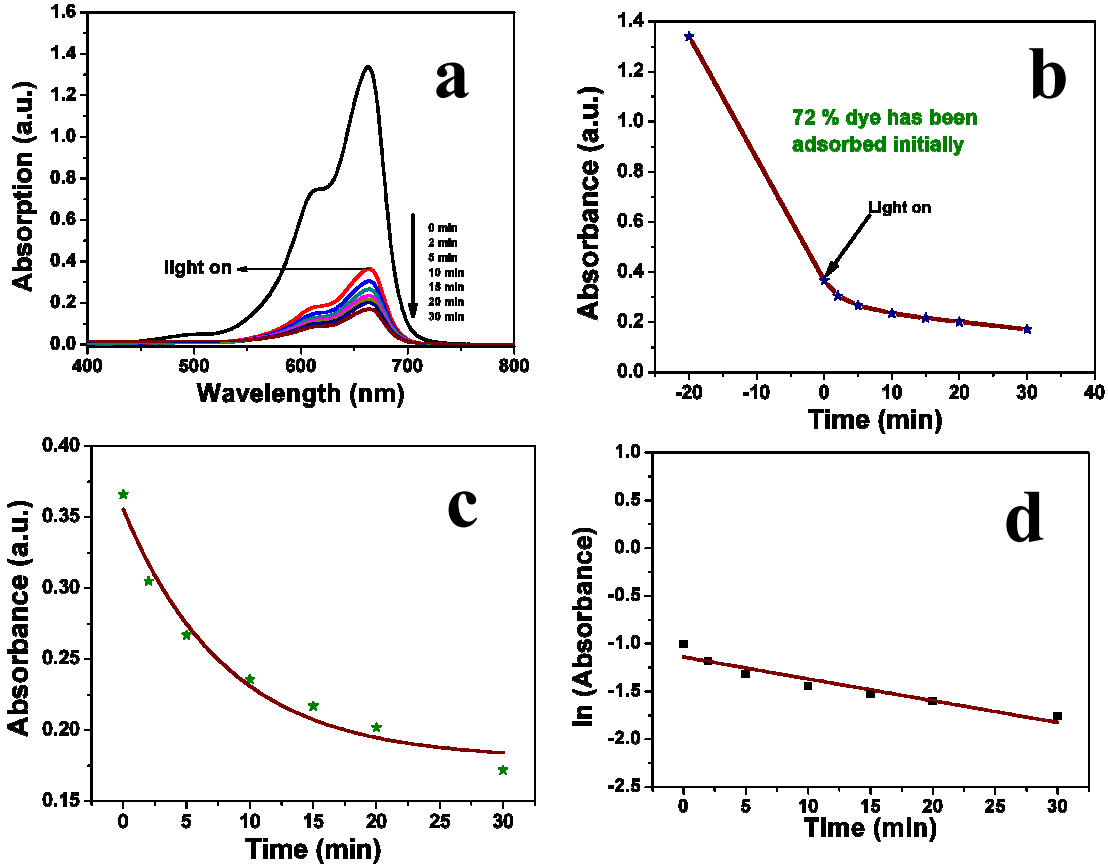

Figure 8: Photocatalytic decomposition of methylene blue by ZnO/CuS (a) plot of absorbance vs. wavelength, (b) plot of absorbance vs. time including adsorption also, (c) plot of absorbance vs. time (only the photocatalysis part), (d) plot of logarithm of absorbance vs. time.

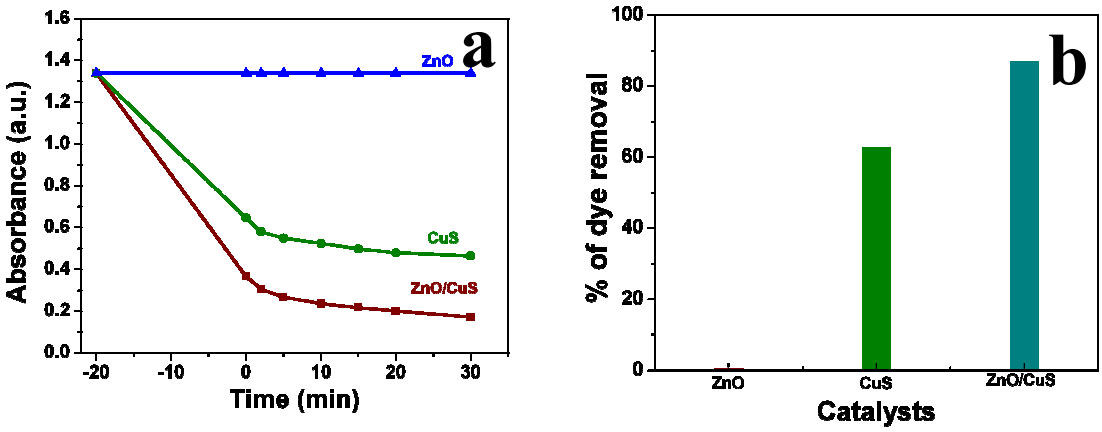

Figure 9: Comparative photocatalytic study of bare ZnO, bare CuS and ZnO/CuS (a) plot of absorbance vs. time (b) bar diagram of % dye removal efficiency.

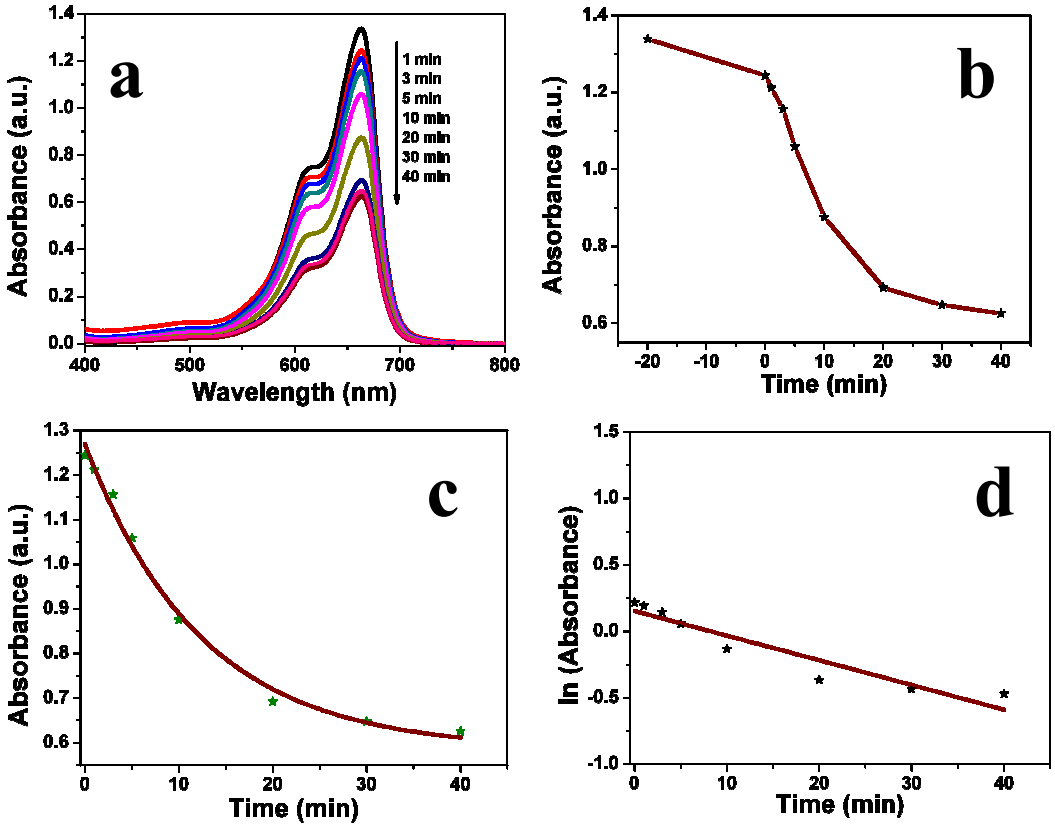

Figure 10: Photocatalytic decomposition of methylene blue by ZnO/CuS in presence of $AgNO_3$ (a) plot of absorbance vs. wavelength, (b) plot of absorbance vs. time including adsorption also, (c) plot of absorbance vs. time (only the photocatalysis part), (d) plot of logarithm of absorbance vs. time.

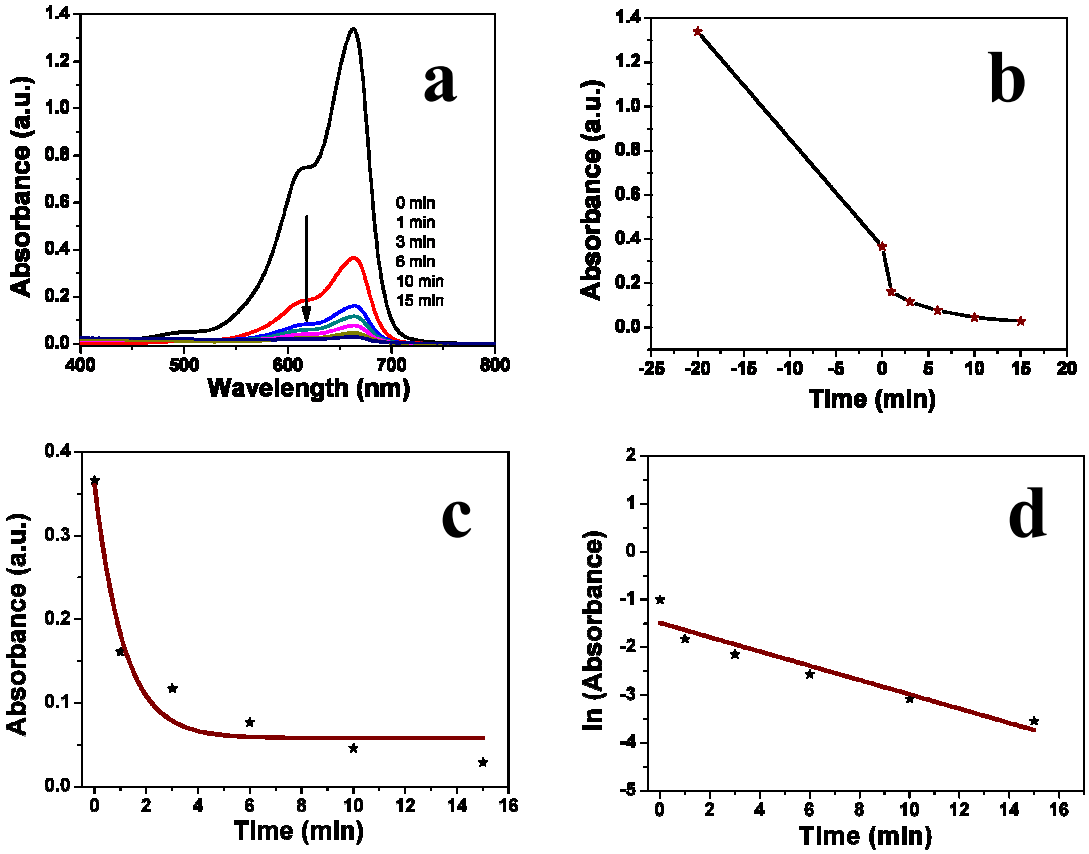

Figure 11: Photocatalytic decomposition of methylene blue by ZnO/CuS in presence of ammonium oxalate (a) plot of absorbance vs. wavelength, (b) plot of absorbance vs. time including adsorption also, (c) plot of absorbance vs. time (only the photocatalysis part), (d) plot of logarithm of absorbance vs. time.

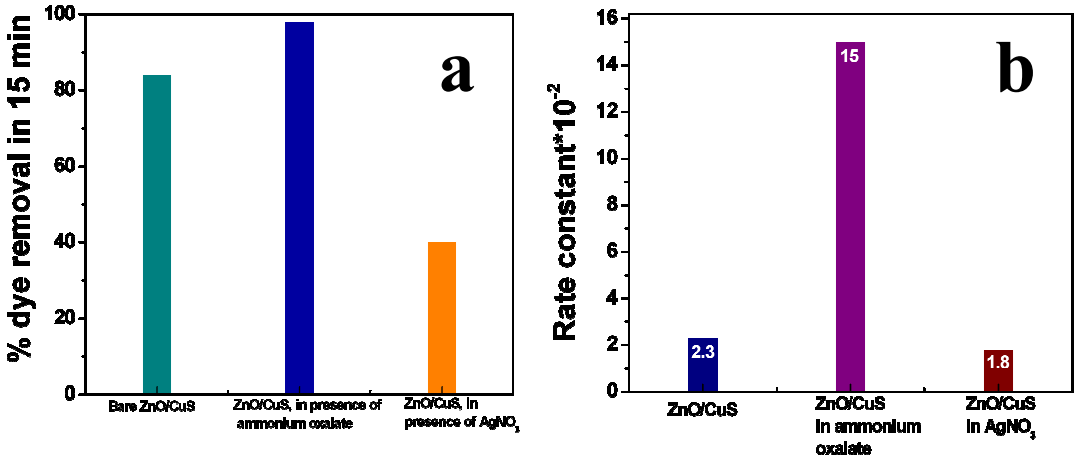

Figure 12: Comparative photocatalytic study of bare ZnO/CuS, ZnO/CuS in presence of ammonium oxalate and silver nitrate (a) bar diagram of efficiency of dye removal, (b) bar diagram of rate constant values.

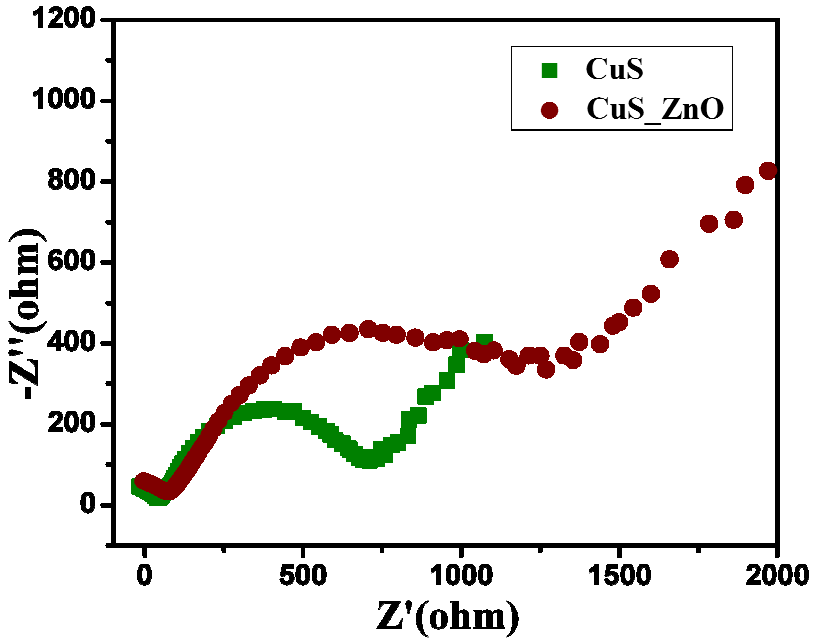

Figure 13: Electrical impedance spectra: Nyquist plot of ZnO/CuS and CuS in dark condition.